

Original Article

Optimal Utilization of Power in a Grid-Interfaced Hybrid Renewable Energy-Powered Electric Vehicle Charging Station with an ATLA-based Controller

Vechalapu Kamaraju¹, Chintapalli V V S Bhaskara Reddy²

^{1,2}Department of Electrical Engineering, Andhra University College of Engineering (A),
Andhra University, Visakhapatnam, Andhra Pradesh, India.

¹Corresponding Author : raju.vechalapu@gmail.com

Received: 26 April 2023

Revised: 05 June 2023

Accepted: 14 June 2023

Published: 25 June 2023

Abstract - Developing a reliable power system model will enable the most efficient use of power in a grid-linked hybrid renewable energy-powered electric vehicle charging station (EVCS). The proposed EVCS model is made by putting together solar PV modules, wind turbines, a series capacitor buck converter (SCBC), a maximum power point tracker (MPPT), a utility grid, a robust controller, and an advanced control architecture. A potential controller is developed using the Artificial Transgender Longicorn Algorithm (ATLA) to enhance the charging station's efficiency by providing optimal switching to the converter. The proposed controller creates a precise and accurate control signal database for the offline mode, which is the transmission of energy from a source to a load. The proposed model is examined under different cases in MATLAB and Simulink, and the performance of EVCS is compared to that of other methods already in place.

Keywords - Electric vehicle charging station, Solar energy, Wind energy, Microgrid, Integrated converter.

1. Introduction

At present, the majority of vehicles are fitted with a range of fuel types, such as gasoline, diesel, petrol, and others. Moving people and goods consumes more than 25% of all energy on the globe, according to figures from the Energy Information Administration [1]. The transportation sector also contributes to the production of greenhouse gases, primarily SO₂ and CO₂. Greenhouse gases cause climate change and global warming. These are currently major concerns since they may negatively impact the Earth's ecology and way of life. The main contributors to climate change are greenhouse gases [2]. In 2021, global energy-associated carbon dioxide pollutants will have grown by 6%, or 36.32 billion tons, according to the global carbon project at COP26 [4]. According to research by Prof. Pierre Friedlstein, to reach net zero CO₂ emissions by 2050, it will be necessary to reduce CO₂ pollutants by an average of 1.4 billion metric tonnes annually. The Center for Science and Environment says that in 2021, India will emit 2.88 billion metric tonnes of CO₂. The goal for India is to have no emissions by 2070.

In order to achieve this target, the nation must cut its overall projected carbon emissions by one billion metric tonnes between now and 2030 and meet half of its total energy demand [5]. Due to the considerable amount of carbon dioxide that conventional automobiles emit into the atmosphere,

electric vehicles (EVs) have recently received a great deal of focus [6]. Demand for imported crude oil and a scarcity of fossil fuels prompted people to seek out less expensive and more environmentally friendly modes of transportation, such as electric cars [7]. Approximately 6.5 million electric vehicles (EVs), including plug-in hybrids and fully electric passenger cars, were sold between 2020 and 2021, representing a 109 percent increase [8]. Tesla accounted for 14% of the worldwide EV market. The rate at which electric cars become more popular could greatly affect how electricity is distributed [9]. The system's stability and power quality are frequently compromised while charging electric vehicles via the public grid [10].

Additionally, the charging burden will be more noticeable when EV charging occurs when the public grid is under the most strain [11]. A list of strategies developed by researchers can help decrease the impact on the utility grid. The best option for decreasing the burden on the utility grid is to install RES-powered EVCSs [12]. Solar and wind energy are the most common energy resources on the globe. Unlimited, affordable electricity might be produced with solar and wind energy. They are environmentally friendly since they are more reliable, durable, and less effective on the environment [28]. The HRES integrated into microgrids can deliver the power expected to satisfy energy demands [14]. The PV and WEC



systems' inconsistent nature directly affects electricity generation [15]. Several studies have been done on power management and energy efficiency in EVCS powered by renewable energy. Some of these studies made me want to do this work. The authors, Ahmed et al. (2022), presented their work on energy management in PV-based EVCS in commercial areas, but if they also included other RES, the EV charging impact on the grid would be reduced more [16]. The author, Alex Caines et al. (2021), presented his work on a PV-assisted intelligent EVCS power station [17]; this work is limited to the solar source and not combined with other sources, and it is independent of the utility grid. The author, Rajendran et al. (2021), plan to schedule power in EVCS with a PSO control strategy, but the control method is competitive, and the execution time is long [18]. In 2021, G. Madhuri et al. created an HRES-powered fast-charging system with a fuzzy controller [19]. It gives a better result but does not give a unique solution. The computational effort required to construct fuzzy rule bases is a significant disadvantage of fuzzy controllers. The authors, Jyothi P. et al., focus on DC charging systems in 2020 [29]. By utilising Res with a simple dc/dc boost converter, they limited the work to only dc charging and did not propose any novel converters for better efficiency. An effective controller and control technique should be needed to track maximum and stable power from the HRES with minimal loss.

In this proposed work, I have overcome all limitations and proposed a novel controller for the proposed HRE-powered EVCS associated with the modified series capacitor buck converter (SCBC) in order to obtain optimal power utilisation [21]. This recommended converter was modelled by adopting the state-space averaging method [22]. The SCBC is investigated, equations are framed by considering its modes of operation, and the voltage transfer gain is derived. The performance and dynamic response of the converter are investigated using small-signal analysis. In this study, in the first stage, we used two MPPT controllers with the popular Perturb & Observe method, one for collecting optimum power from a PV system and the other for collecting optimum power from wind energy [23]. In the second stage, we designed a controller with the Artificial Transgender Longicorn Algorithm for optimal switching for grid-side inverters [24]. In MATLAB-Simulink, the performance of the ATLA control technique is compared with other methods in the literature to see how well it works. The HRE-based EVCS is examined in different cases, like source variations and load variations. In all cases, the responses were looked at and compared to existing methods like AGOA [25] and GWO [26].

The remaining work is detailed as follows: The grid-interfaced HRE-powered EVCS with an ATLA controller structure is detailed in Section 2. The modelling and design of the modified SCB converter, as well as its operating modes, are detailed in Section 3. The current work's control mechanism is briefly detailed in Section 4. The findings from

MATLAB and Simulink are analysed in Section 5. The present work is concluded in Section 6.

2. The Model of the HRE-based EVCS

The suggested grid-interfaced HRE-powered EVCS model is shown in Figure 1. The suggested EVCS model is a combination of solar PV systems, wind energy conversion systems, SCBC, MPPT, ATLA-controller, DC-Microgrid, grid, and electrical charging points.

2.1. Location of Grid-Interfaced HRE-based EVCS

The generation of electrical power by using renewable energy sources depends on the location of the site where the plant is installed. The power generation with a PV system depends on solar irradiance, and the power generation with WECS depends on wind speed. The solar irradiance, solar peak hours, and wind speed will vary from place to place. Correspondingly, the power generation by RES also varies. This work considered the EVCS installed in Visakhapatnam, India. Visakhapatnam is north of the equator [1, 3]. It gets an average of 5 to 5.5 kWh/m²/day of solar radiation every day, and the average wind speed is about 15 km/h or 4.166 m/s.

2.2. Load Estimation and Design Considerations

In this work, it used a 12 KW grid-connected HRE-powered EVCS model for the EVs of university employees in the department parking lot. To determine the electric load, look at the battery sizes of a few electric scooters and cars. The staff can use EVCS for only eight hours each day, even if it takes the vehicle battery longer to charge to its full capacity. Then the power consumed by the EV is calculated as below:

$$\text{Energy drawn} = \frac{\text{Charging Period (h)}}{\text{Rated charging period (h)}} \times \text{Battery Capacity (KWH)}$$

In table.1, considered the total load on the grid-connected HRE-powered EVCS to be 288.13 KWH per day. Every day, the HRE system tries to match the generation with the load. The power generation with a solar PV system depends on the sun's peak hours, and the WECS depends on wind speed. The load on the EVCS is almost minimal when the institution is closed, and electricity produced by the HRES is fed into the grid via net metering. When the EVCS is heavily loaded, it will use grid power.

2.3. Charging Methods and Power Ratings

DC power is required to charge an EV's battery pack. However, the power lines from the utility grid distribute AC power. So, a rectifier unit is necessary to convert AC to DC and send DC power to the battery. In EVCS, Either AC or DC can be used to do conductive charging. If an AC EVSE is used, then the EV's onboard charger is required for changing AC power into DC. If a DC EVSE is used, then the EV's onboard charger is not required. There are four modes of charging available for EVs. The first three charging modes are AC charging, while mode 4 is DC charging.

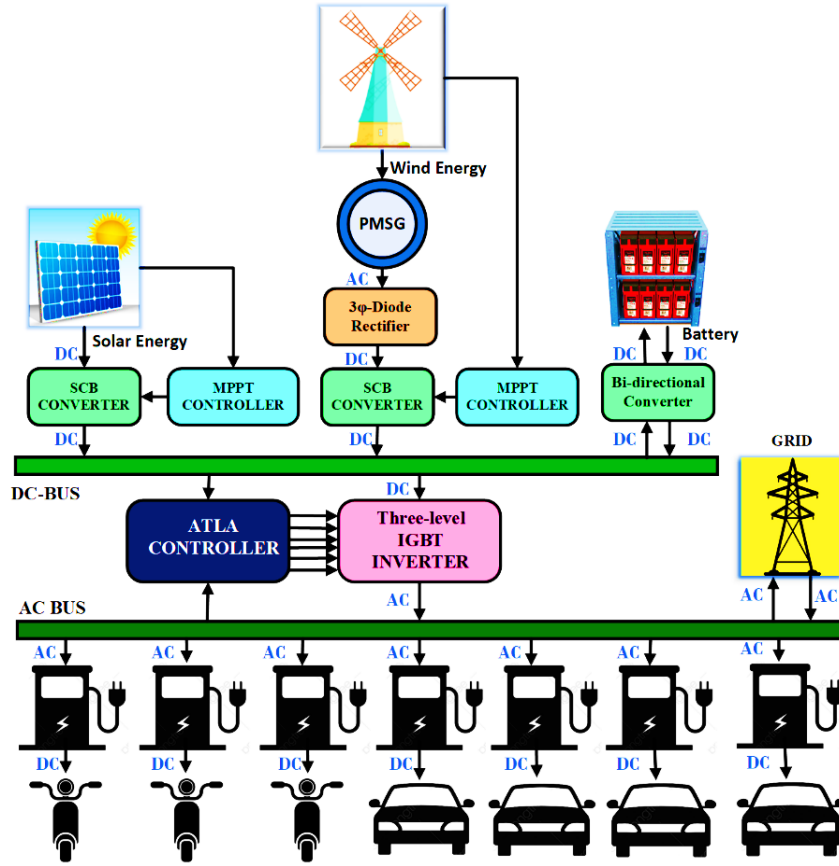


Fig. 1 The architecture of the HRE-based EVCS

Table 1. Load estimation and design considerations

S. No	EV models	Battery Capacity (KWH)	Rated Charging period (H)	Charging period (H)	Qty	Load on EVCS per day (KWH)
1.	MG ZS EV	44.5	7	7	1	44.50
2.	Hyundai Kona	39.2	6.16	6.16	1	39.20
3.	Tata Nexon EV	30.2	9.16	8	1	26.37
4.	Tata Tigor EV	26	8.75	8	1	23.77
5.	Mahindra eVerito	21.2	11.5	8	2	29.49
6.	Ather 450X	2.7	5	5	10	27
7.	Simple One	4.8	2.75	2.75	11	52.8
8.	Bajaj Chetak	3	5	5	15	45
Total Load on EVCS per day						288.13

Table 2. Charging methods and power ratings

Type of Charging	Power Range	Charging Type	Compatible Vehicles
Regular charging (Low power)	$P \leq 7 \text{ KW}$	DC & AC	E-2Ws, E-3Ws, E-Cars other LCVs (up to 1 ton)
	$7 \text{ KW} \leq P \leq 22 \text{ KW}$	DC & AC	
Powerful charging (High power)	$22 \text{ KW} \leq P \leq 50 \text{ KW}$	DC	E-Cars, LCVs and MCVs (1-6 tons)
	$50 \text{ KW} \leq P \leq 200 \text{ KW}$	DC	

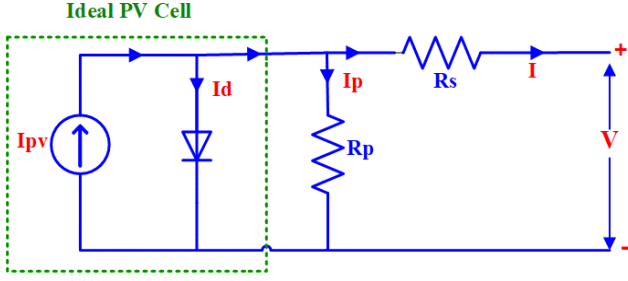


Fig. 2 Circuit diagram of photovoltaic cell

Table 2 categorizes different types of EV charging based on their power output; low-power charging is restricted to 22 kW, while high-power charging is limited to 200 kW. Most EVSEs that can handle up to 500 kW of power are good for large trucks and buses.

3. Modelling of HRE-powered EVCS

The first and foremost task in the design of HRE-powered EVCS is modelling. The PV system is modelled according to its load share. The wind turbine is modelled according to the required mechanical output. The PMSG is to be modelled according to the required electrical power generation. The converter is modelled according to our required output voltage. The controller is modelled to get optimal switching of the converter. That optimal switching enhances the system's efficiency.

3.1. Photovoltaic Cell Modelling

An ideal photovoltaic cell is designed by connecting a freewheeling diode in a shunt manner with a current source, according to Figure 2.

$$\tilde{I}_{pv} = [\tilde{I}_{sc} + K_I(T - T_{ref})] \frac{G}{G_{ref}} \quad (1)$$

$$\tilde{I}_{sat} = \tilde{I}_{rs} \left[\frac{T_c}{T_{ref}} \right]^3 \text{Exp} \left[\frac{qE_g}{nk} \left(\frac{1}{T_{ref}} - \frac{1}{T_c} \right) \right] \quad (2)$$

$$\tilde{I} = \tilde{I}_{pv} - \tilde{I}_{sat} \left[\text{Exp} \left(\frac{V + \tilde{I}R_s}{nV_T} \right) - 1 \right] - \left[\frac{V + \tilde{I}R_s}{R_{sh}} \right] \quad (3)$$

Where, \tilde{I}_{pv} is the photocurrent calculated as shown in the equation.1, \tilde{I}_{sat} is the cell saturation Current is calculated as shown in equation.2.

3.2. Modelling of the Wind Turbine

A wind turbine's mechanical output, also known as torque, is influenced by several elements, such as wind speed, turbine size, and design. The mechanical output of a wind turbine is mathematically modelled in terms of air density (ρ), the radius of the blade (R) in meters, swept area of the wind turbine (A), power coefficient $C_p(\lambda, \beta)$, and the mechanical output power is calculated as shown in Equation 4.

$$P_m = \frac{1}{2} * \rho * A * C_p(\lambda, \beta) * V^3 \quad (4)$$

The power coefficient $C_p(\lambda, \beta)$ can be determined in terms of Tip speed ratio (λ) and pitch angle (β) in degrees, as shown in equation 5.

$$C_p(\lambda, \beta) = \frac{1}{2} \left[\frac{116}{\lambda_i} - 0.4\beta - 5 \right] e^{-\frac{21}{\lambda_i}} \quad (5)$$

$$\frac{1}{\lambda_i} = \frac{1}{\lambda + 0.08\beta} - \frac{0.035}{1 + \beta^3} \quad (6)$$

$$\lambda = \frac{\omega R}{V} \quad (7)$$

The optimal power is obtained from the WECS by maintaining all values, including rotational speed. Here, the optimal value for the coefficient of power is 0.59, the speed ratio of the tip is 6 to 8, and the air density is 1.2 kg/m². The optimal power is calculated as shown in equation 8.

$$P_{optimal} = K_{optimal} * \omega_{optimal}^3 \quad (8)$$

3.3. Modelling of the Generator

The two-phase synchronous reference frame (SRRF) concept is the basis for the modelling of PMSG. In this concept q-axis and the d-axis are having phase difference is 90 degrees. In a synchronous reference frame, the following equations provide the electrical model of PMSG:

$$\frac{di_d}{dt} = -\frac{R_a}{L_d} i_d + \omega_e \frac{L_q}{L_d} + \frac{1}{L_d} u_d \quad (9)$$

$$\frac{di_q}{dt} = -\frac{R_a}{L_q} i_q - \omega_e \left(\frac{L_d}{L_q} + \frac{1}{L_d} \right) + \frac{1}{L_d} u_q \quad (10)$$

$$\omega_e = P\omega_g ; e_q = \omega_e \lambda_o \quad (11)$$

$$T_e = 1.5 P [(L_d - L_q) i_d i_q + i_q \lambda_o] \quad (12)$$

where, ' R_a ' is the resistance of stator winding, ' ω_e ' is the rotating speed in electrical degrees, ω_d is the rotating speed in mechanical degrees, P is the number of pair of poles, u_d and u_q are d and q-axis voltages, L_d and L_q are the d and q axis inductances, ' T_e ' is the electromagnetic torque calculated as shown in equation 13.

3.4. Modelling of the Modified SCB dc-dc Converter

The SCB DC/DC Converter belongs to the interleaved buck converter (IBC) family; those converters are mainly used in industries for high-power applications. The interleaved approach enhances converter dynamics while reducing input and output filter requirements. Both switches must be closed for maximum voltage conversion. The two inductor currents (i_{L1} and i_{L2}) must be balanced in a unique way for them to be equal. Kisu Kim et al. (2017) developed the SCBC to resolve the issues with the conventional IBC [21]. Have made a few modifications to the converter, which have been used in this

proposed system model. The SCBC is effective in addressing the problem of voltage stress at startup. When both switches are open, capacitors (C_1 and C_2) are linked in series, and the circuit is parallel to the source, causing $v_{C1} + v_{C2} = v_{in}$. The recommended converter is developed in the manner seen in Figure 3.

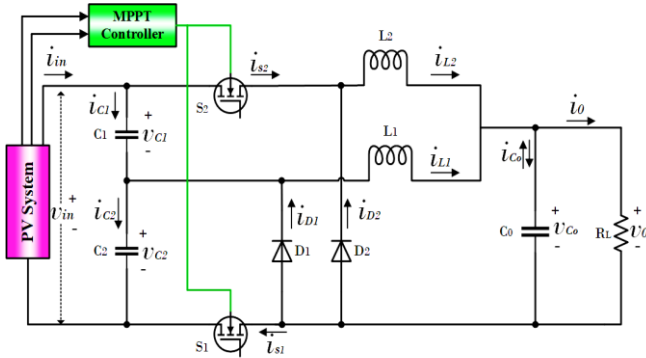


Fig. 3 Circuit diagram of the modified SCBC

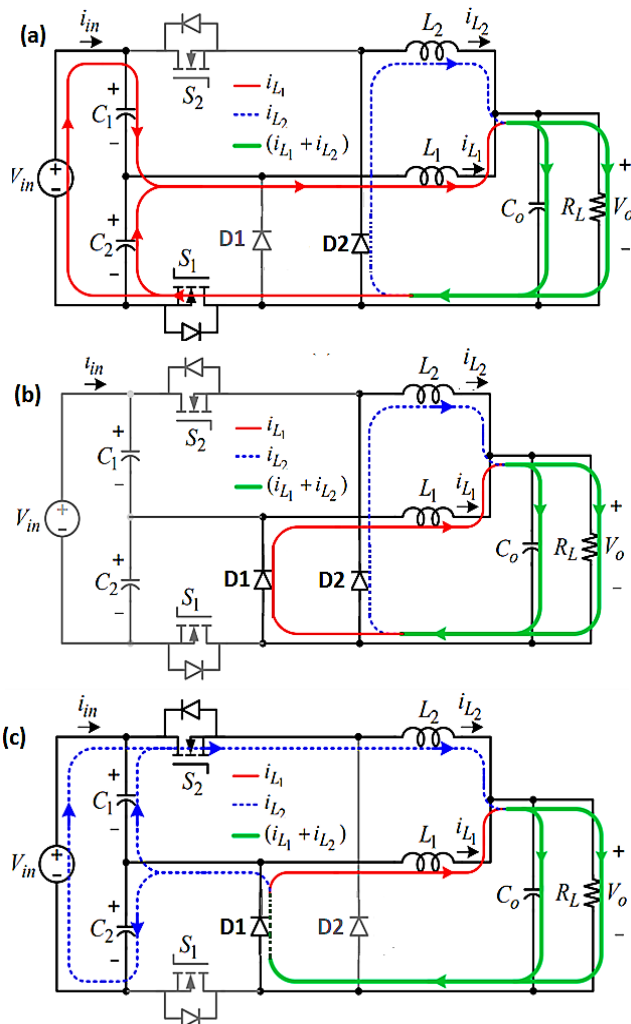


Fig. 4 The operating modes of a modified SCB converter

In order to maintain steady switch voltages, the capacitors are later discharged. The two capacitors are referred to as C_1 and C_2 , respectively, because it is simpler just to consider their capacitance values to be equal. The voltage across each capacitor is also the same and equal: $v_{C1} = v_{C2} = v_{in}/2$. The proposed modified SCBC was investigated using its operational modes, and its operation is similar to the standard SCBC.

3.4.1. The Operating Modes of a Modified SCB Converter

The operating modes are succinctly outlined below;

Mode I

In this mode, Switch S1 is operating in the ON position, Switch S2 is operating in the OFF position, Diode D1 is not in the mode of conduction, and Diode D2 comes into conducting mode as shown in Figure 4a

Mode II

In this mode, both S1 and S2 are turned off, and then the load circuit becomes a source-free circuit, as shown in Figure 4b. D1 and D2 diodes are both conducting. The inductor currents (i_{L1} and i_{L2}) are circulated through the diodes D1 and D2, respectively. There is hardly any current passing through the capacitors.

Mode III

The S2 is turned on while the S1 is turned off, and diode D1 comes into conducting mode, but diode D2 is not in conduction, as shown in Figure 4c.

3.4.2. Voltage Transfer Gain (V_{Tg})

Equation 14 illustrates how to get the voltage transfer gain for the recommended converter from the voltages of the inductors. This is how it works:

$$(0.5V_{in} - V_{out})dT_s = V_{out}(1 - d)T_s \tag{13}$$

$$V_{Tg} = \frac{V_{out}}{V_{in}} = \frac{d}{2} \tag{14}$$

where V_{in} is the input voltage and V_{out} is the output voltage, respectively, while "d" refers to the converter's duty ratio.

3.5. Modelling of the Bi-directional Converter

The bidirectional converter evolved from a unidirectional converter, allowing energy to flow in both directions. Those converters control the energy flow in both directions from the energy storage unit to the DC microgrid and vice-versa.

When the voltage of the DC bus is greater than the voltage of the battery, the bi-directional converter switches into charging mode. Equation 15 illustrates how to describe the bidirectional converter's voltage conversion ratio while it is in charging mode (bucking mode):

$$\frac{V_B}{V_{DC}} = \frac{T_{S1 ON}}{T_{S1 ON} + T_{S1 OFF}} = D \quad (15)$$

When the voltage of the DC bus is less than the battery voltage, the bi-directional converter switches to the discharging mode. Equation 16 illustrates how to describe the bidirectional converter's voltage conversion ratio while it is in discharging mode (boosting mode):

$$\frac{V_B}{V_{DC}} = \frac{T_{S2 ON} + T_{S2 OFF}}{T_{S2 OFF}} = \frac{1}{1-D} \quad (16)$$

3.6. Modelling of the Controller

A robust controller with excellent control methods is required to make the system more efficient by managing power in the best way. In this, recommended an ATLA-based controller for achieving optimal power management and high system efficiency. In the design process, modelling is a foundation task. Here, the main object of the controller is to minimize the error by tuning the gains of the PI controller. The control structure is described briefly in Figure 6. It is as follows:

At first, the controller senses the three-phase voltage (V_{abc}) and three-phase current (I_{abc}) from the grid, and then it transforms those values into $\alpha\beta$ - frame by using Park's transformation. After that, it again transforms into the two-phase synchronous reference frame (dq - frame) using Clark's transformation. In order to continue synchronization among the three phases and the d-q rotating reference frame, a phase-locked loop is employed. The errors in the active component of current and the reactive component of current are presented in Equation 17. The active and reactive components of voltages are computed as shown in Equation 18. The voltage references are obtained as shown in Equation 19. Here I_d, I_q are the active and reactive components of current; similarly, V_d, V_q are the active and reactive components of voltage.

$$I_{d_error} = I_d^* - I_d; \quad I_{q_error} = I_q^* - I_q \quad (17)$$

$$E_d = (K_p + \frac{K_i}{s})I_{d_error}; \quad E_q = (K_p + \frac{K_i}{s})I_{q_error} \quad (18)$$

$$v_d^* = v_d + (E_d + \omega LI_q); \quad v_q^* = v_q + (E_d - \omega LI_d) \quad (19)$$

where the (*) indicates reference values, "ω" is the grid frequency, and "L" is the inductance of the filter. These two-phase dq-reference voltages are transformed into three-phase reference voltages for the PWM unit to generate optimal switching for the voltage source inverter.

4. Implementation of the ATLA Approach

This section gives a brief description of the ATLA method, which is a new metaheuristic optimization method [19]. The long-tail characteristic of search is what inspired the

efficient optimization technique. The male longicorn looks for a mate, but the female longicorn makes it easier for the male by putting out a sex pheromone. Those in the concentration zone will detect the pheromone and migrate in the direction of Fermina by taking the shortest route. The program conversed with minimum time and gave an optimal solution faster than other optimization algorithms. Figure 5 depicts the movement of a male longicorn in response to the detection of a sex pheromone released by the Fermina.

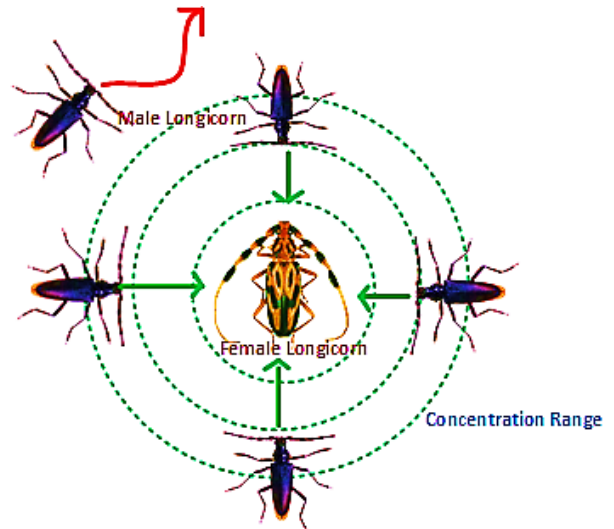


Fig. 5 Diagram of Fermina's sex pheromone concentration range

4.1. Procedural steps of ATLA for getting the Optimal Solution

- Step 1: Parameter Initialization
Initialize all the program's parameters in this step, including p, q, s, α, λ, and T. The step control quantity (α) is set to 1 in this phase, and the population size is taken to be n.
- Step 2: Random Generation
Once setup is complete, create input parameters at random to provide the best outcome.
- Step 3: Establishing Objective Function
In this step, define the objective function as an error minimization function, as shown in equation 20.

$$C = \min \{e(t)\} \quad (20)$$

where $e(t) = (K_p + \frac{K_i}{s})I_{d_error}$; (or) $(K_p + \frac{K_i}{s})I_{q_error}$

- Step 4: Attraction Movement
In this stage, the male longicorn begins to look for a high fitness value in accordance with the objective function. In order to attract the attention of a male longicorn, the transgender longicorn must alter its gender, settle down, and release sex pheromones.

The longicorn they scented was a male, and it went toward Fermina. The formula for a male longicorn's ideal journey distance is as shown in equation 21:

$$\vec{d}_i = \frac{z_{best}^t - z_i^t}{\|z_{best}^t - z_i^t\|}; \quad i=1,2,3,\dots,p \quad (21)$$

where, "t" denotes the current iteration number;" Z_i^t " denotes the jth male position; " Z_{best}^t " is the female position, indicating the place of greatest fitness in the current herd, and "p" denotes the maximum number of male longicorns that may be concentrated in each area.

Step 5: Updating Position

In this step, the longicorn positions are updated according to the concentration of sex pheromone as shown in equation 22:

$$Z_i^{t+1} = Z_i^t + S_i^t \times \vec{d}_i^t \quad i=1,2,3,\dots,p \quad (22)$$

Where, S_i is the moving step length of the i^{th} male longicorn.

Step 6: Updating Step Size

In this step, the longicorn's step size is updated according to the fitness value number of iterations is varied with respect to desired step size as shown in equation 23.

$$S_i^t = \frac{0.95 \times S_i^{t-1}}{r_i} \quad (23)$$

Where, r_i is the i^{th} male longicorn's rank of fitness.

Step 7: Random Search in Variable Space

The male longicorn outside of Fermina's concentration zone will not be able to feel the sex phenomenon she releases. They were unable to alter their postures. Randomly scanning the area, they eventually arrived at the concentration area, as depicted below in Equation 24.

$$Z_i^{t+1} = Z_i^t + \alpha \oplus L(\lambda) \quad ; i=1, 2\dots p-q-1 \quad (24)$$

Where " α " equals 1 as the advanced step value; "p" is the population size of the longicorn; " \oplus " is the step-by-step multilocational operator; $L(\lambda)$ is a random movement.

Step 8: Obtain optimal values

The male longicorn reached Fermina by travelling the optimal distance \vec{d}_i with Z_{best} and obtain optimal function value.

5. MATLAB/Simulink Results and Analysis

Optimal utilization of power and energy management in the grid-interfaced HRES-powered EVCS associated with the modified SCBC is demonstrated in this. The ATLA controller is introduced. In this instance, the ATLA controller produces an accurate control signal to ensure the best possible energy management for optimal utilization of EVCS. The system's output is used to judge how well the proposed system works with the ATLA control scheme. The system is also tested with several other control schemes.

5.1. Case 1: Changing Solar Irradiation and Wind Speed Under Constant Load

The HRE-powered EVCS in Case 1 is operated at constant load conditions with varying solar irradiation and wind speed. Figure 6(a) shows that the Changing Figure 6(b) depicts the changing wind speed at and near 15 km/h.

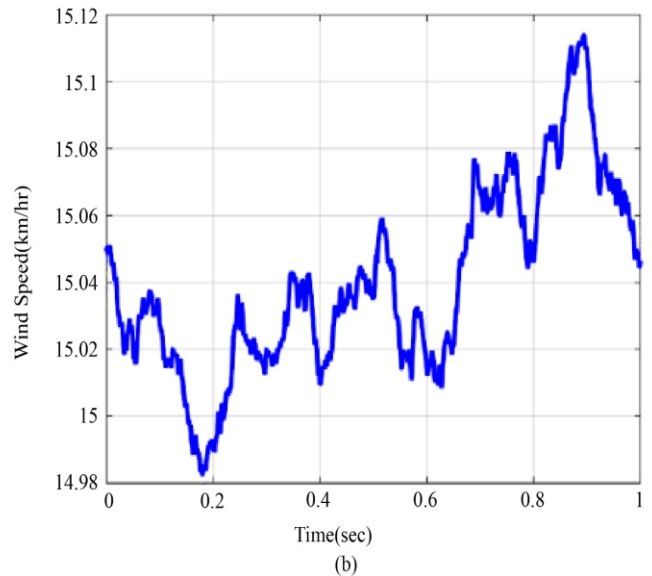
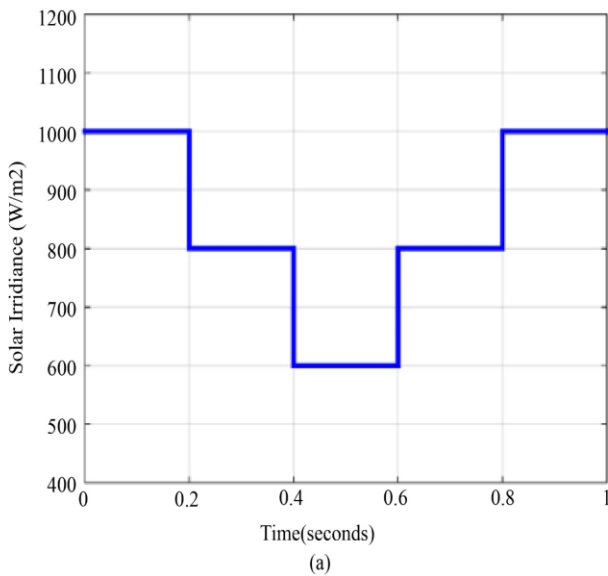


Fig. 6 Variation of sources (a) PV irradiance, (b) Wind speed

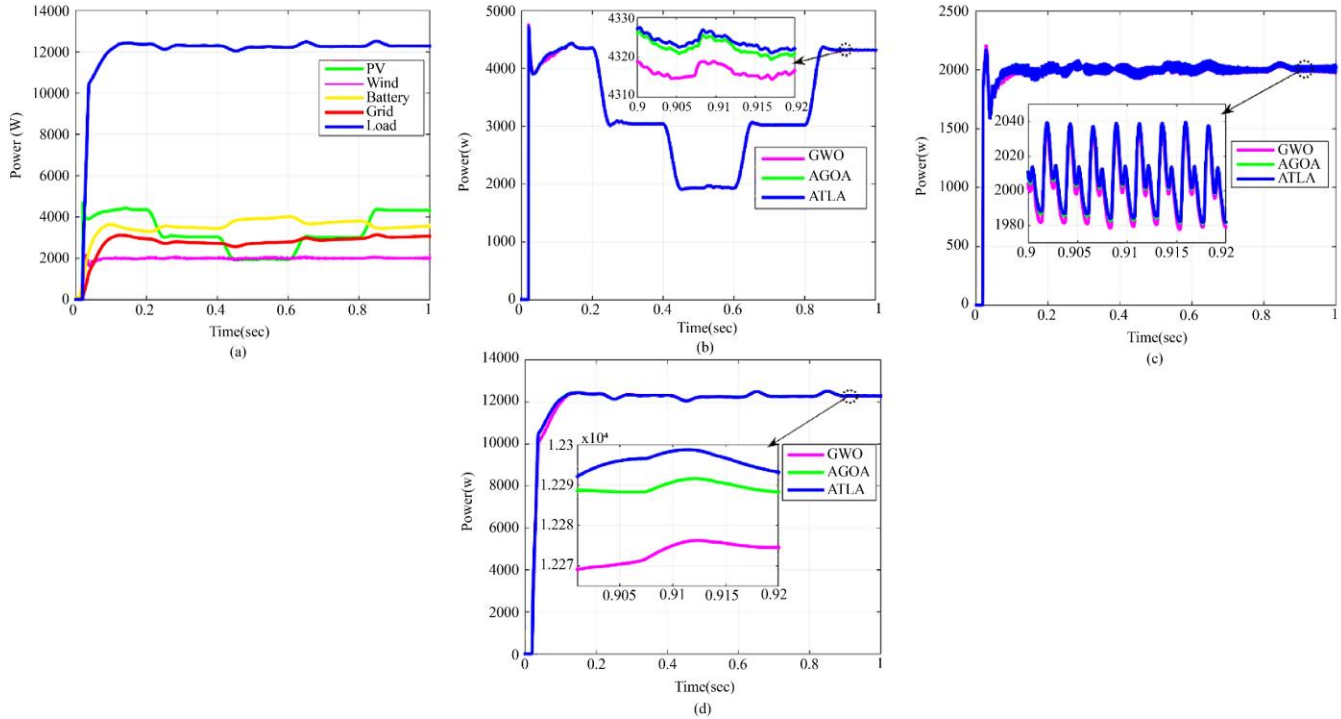


Fig. 7 Power outcomes under case-1 (a) Load Sharing (b) PV power, (c) Wind power, (d) load power

Figure 7 shows load sharing and a comparison of power at source and load using a suggested controller made with the ATLA technique versus other current methods like AGOA and GWO in Case 1. Figure 7 (a) shows the sharing of load between energy sources. The total load on the model is 12294 W, of which PV contributed 4320 W, the wind source contributed 2027 W, the battery provided 3558 W, and the grid supplied 3072 W. Figure 7 (b) shows the comparison of the power tracking from a PV source with current and recommended approaches. The greatest power obtained in the system using the GWO technique was 4320 W. The greatest power obtained using the AGOA technique in the system was 4324 W. The greatest power obtained in the system using the ATLA technique was 4328 W. The recommended system with the recommended ATLA-based controller achieved a high output power in this observation. Figure 7 (c) shows the comparison of the power tracking from wind energy with current and recommended approaches. The greatest power obtained in the system using the GWO technique was 2000 W. The greatest power obtained in the system using the AGOA technique was 2005 W. The greatest power obtained in the system using the ATLA technique was 2010 W. The recommended system with the recommended ATLA-based controller achieved a high output power in this observation. Figure 7 (d) shows the evaluation of the load power with current and recommended strategies. The greatest power obtained in the system using the GWO technique was 12270W. The greatest power obtained in the system using the AGOA technique was 12288W. The greatest power obtained in the system using the ATLA technique was 12294 W. The

recommended system with the recommended ATLA-based controller achieved a high output power in this observation. From the observation of case-1 results, the utilization power in an EVCS is improved with the proposed ATLA control technique compared with other existing control techniques. Correspondingly, the efficiency of EVCS is also enhanced with the proposed ATLA controller.

5.2. Case 2: Changing Solar Irradiation Under Constant Wind Speed and Load

Case 2 represents a grid-interfaced HRE-powered EVCS operated at changing solar irradiation at constant wind speed and load.

Figure 8 shows load sharing and a comparison of power at source and load using a suggested controller made with the ATLA technique versus other current methods like AGOA and GWO in Case 2. Figure 8 (a) shows the sharing of load between energy sources. The total load on the model is 12290 W, of which PV contributed 4320 W, the wind source contributed 1994 W, the battery provided 3578 W, and the grid supplied 3087 W. Figure 8 (b) shows the comparison of the power tracking from a PV source with current and recommended approaches. The greatest power obtained in the system using the GWO technique was 4318 W. The greatest power obtained using the AGOA technique in the system was 4324 W. The greatest power obtained in the system using the ATLA technique was 4328 W. The recommended system with the recommended ATLA-based controller achieved a high output power in this observation.

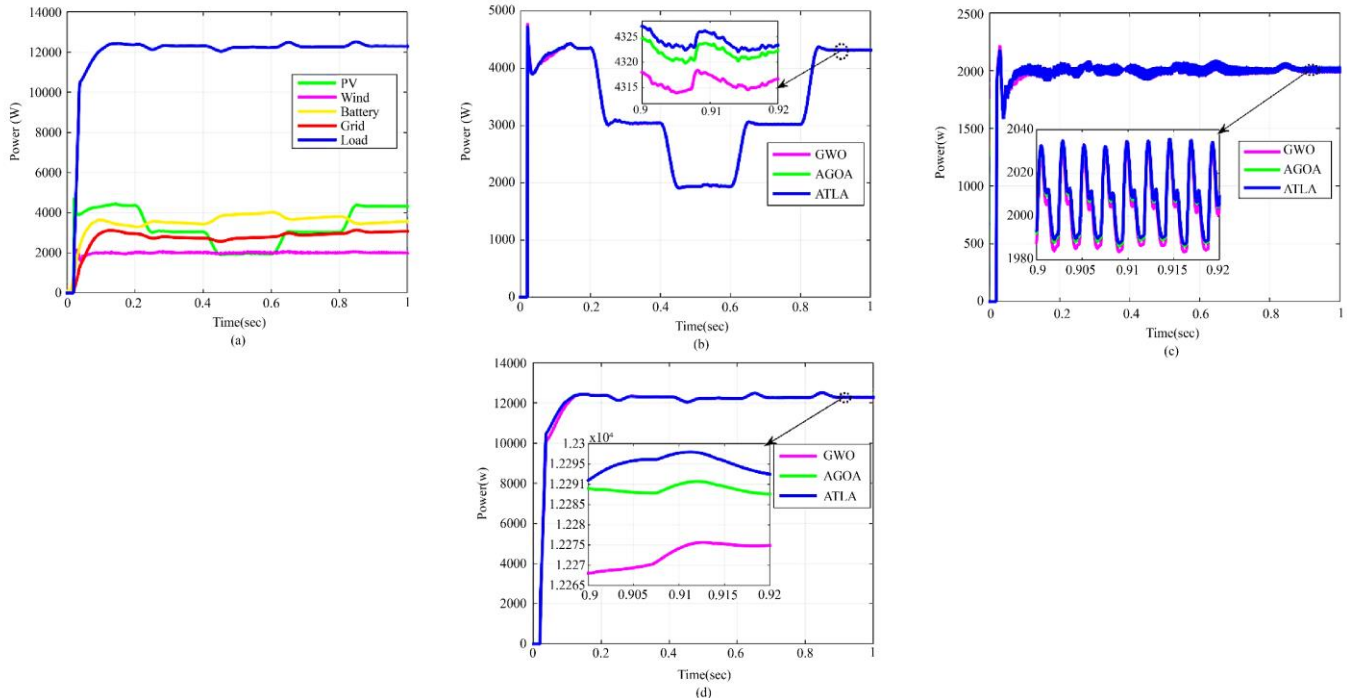


Fig. 8 Power outcomes under case-2 (a) Load Sharing (b) PV power, (c) Wind power, (d) load power

Figure 8 (c) shows the comparison of the power tracking from wind energy with current and recommended approaches. The greatest power obtained in the system using the GWO technique was 1986 W. The greatest power obtained in the system using the AGOA technique was 1988 W. The greatest power obtained in the system using the ATLA technique was 1992 watts. The recommended system with the recommended ATLA-based controller achieved a high output power in this observation. Figure 8 (d) shows the evaluation of the load power with current and recommended strategies. The greatest power obtained in the system using the GWO technique was 12268 W. The greatest power obtained using the AGOA technique in the system was 12288 W. The greatest power obtained in the system using the ATLA technique was 12292 W. The recommended system with the recommended ATLA-based controller achieved a high output power in this observation. From the observation of case-2 results, the utilization power in an EVCS is improved with the proposed ATLA control technique compared with other existing control techniques. Correspondingly, the efficiency of EVCS is also enhanced with the proposed ATLA controller.

5.3. Case 3: Changing Wind Speed Under Constant Solar Irradiation and Load

Case 3 represents the recommended system operated at changing wind speeds at constant solar irradiance and load.

Figure 9 shows load sharing and compares power at source and load using a suggested controller made with the ATLA technique versus other current methods like AGOA and GWO in Case 1. Figure 9 (a) represents the sharing of load

between energy sources. The total load on the model is 12290 W, of which PV contributed 4320 W, the wind source contributed 2027 W, the battery provided 3558 W, and the grid supplied 3072 W. Figure 9 (b) represents the comparison of the power tracking from a PV source with current and recommended approaches. The greatest power obtained in the system using the GWO technique was 4288 W. The greatest power obtained in the system using the AGOA technique was 4295 W. The greatest power obtained in the system using the ATLA technique was 4298 W. The recommended system with the recommended ATLA-based controller achieved a high output power in this observation. Figure 9 (c) represents the comparison of the power tracking from wind energy with current and recommended approaches. The greatest power obtained in the system using the GWO technique was 2000 W. The greatest power obtained in the system using the AGOA technique was 2004 W. The greatest power obtained in the system using the ATLA technique was 808 W. The recommended system with the recommended ATLA-based controller achieved a high output power in this observation. Figure 9 (d) represents the evaluation of the load power with current and recommended strategies. The greatest power obtained in the system using the GWO technique was 12280 W. The greatest power obtained using the AGOA technique in the system was 12296 W. The greatest power obtained in the system using the ATLA technique was 12299 W. The recommended system with the recommended ATLA-based controller achieved a high output power in this observation. From the observation of case-3 results, the utilization power in an EVCS is improved with the proposed ATLA control technique compared with other existing control techniques.

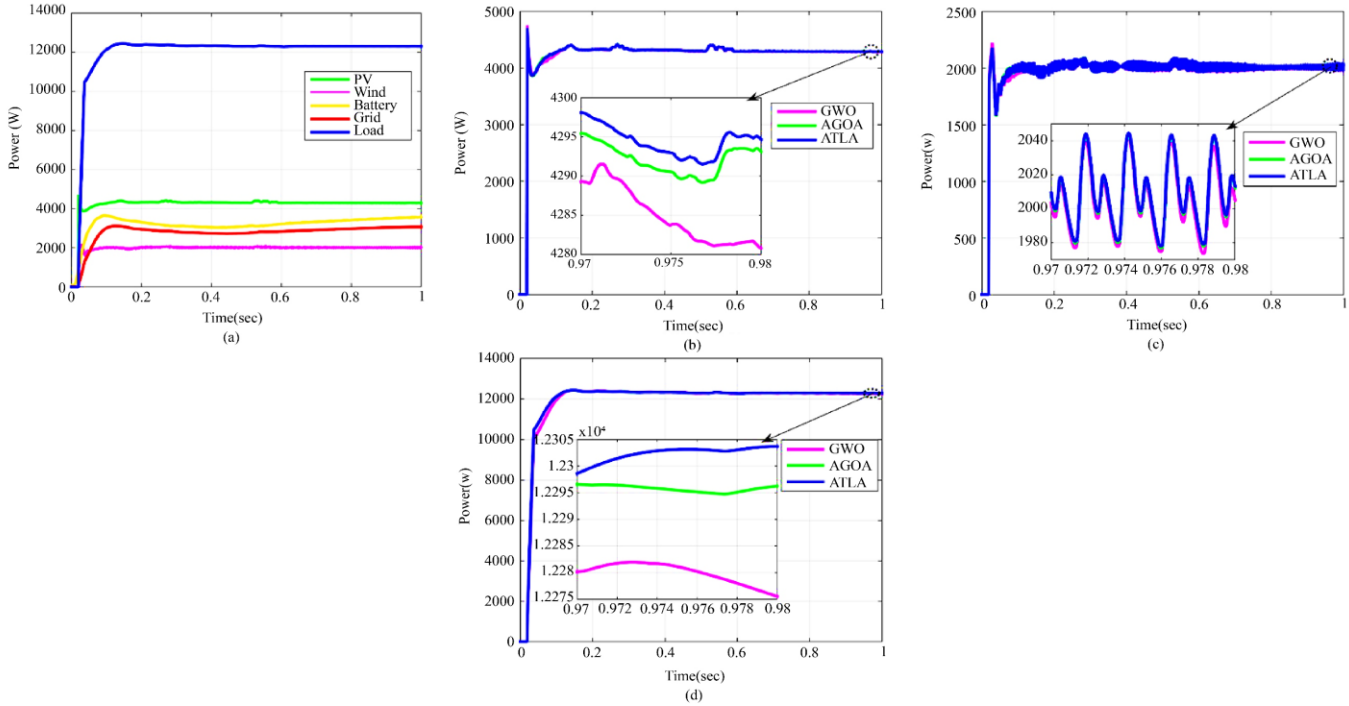


Fig. 9 Power outcomes under case-3 (a) Load Sharing (b) PV power, (c) Wind power, (d) load power

Correspondingly, the efficiency of EVCS is also enhanced with the proposed ATLA controller.

5.4. Case 4: Changing Load Under Constant Solar Irradiation and Wind Speed

Case 4 represents the recommended system operated at changing load at constant solar irradiance and wind speed. Figure 10 shows load sharing and a power comparison at source and load, using a suggested controller made with the ATLA technique versus other current methods like AGOA and GWO in Case 1.

Figure 10 (a) represents the sharing of load between energy sources. The total load on the model is 12440 W, of which PV contributed 4287 W, the wind source contributed 1994 W, the battery provided 3758 W, and the grid supplied 3056 W.

Figure 10(b) represents the comparison of the power tracking from a PV source with current and recommended approaches. The greatest power obtained in the system using the GWO technique was 4283 W. The greatest power obtained using the AGOA technique in the system was 4287 W. The greatest power obtained in the system using the ATLA technique was 4289 W. The recommended system with the recommended ATLA-based controller achieved a high output power in this observation.

Figure 10 (c) represents the comparison of the power tracking from wind energy with current and recommended approaches. The greatest power obtained in the system using

the GWO technique was 2020 W. The greatest power generated by the system using the AGOA technique was 2025 W. The greatest power obtained in the system using the ATLA technique was 2030 W. The recommended system with the recommended ATLA-based controller achieved a high output power in this observation.

Figure 10(d) represents the evaluation of the load power with current and recommended strategies. The greatest power obtained in the system using the GWO technique was 12428 W. The greatest power obtained using the AGOA technique in the system was 12448 W. The greatest power obtained in the system using the ATLA technique was 12456 W. The recommended system with the recommended ATLA-based controller achieved a high output power in this observation. From the observation of case-4 results, the utilization power in an EVCS is improved with the proposed ATLA control technique compared with other existing control techniques. Correspondingly, the efficiency of EVCS is also enhanced with the proposed ATLA controller.

Figure 11 illustrates the tendency for convergence of the control strategies. Subplot 11(a) shows the tendency for convergence of the ATLA control strategy when applied to minimize the error in the objective function. It converged at 0.7027 after 28 iterations. Subplot 11 (b) shows the comparison of convergence characteristics. This subplot taught us that the ATLA control approach converges more quickly than the other two strategies and performs better overall. The fitness values for the AGOA and GWO are 0.7581 and 0.8011, respectively.

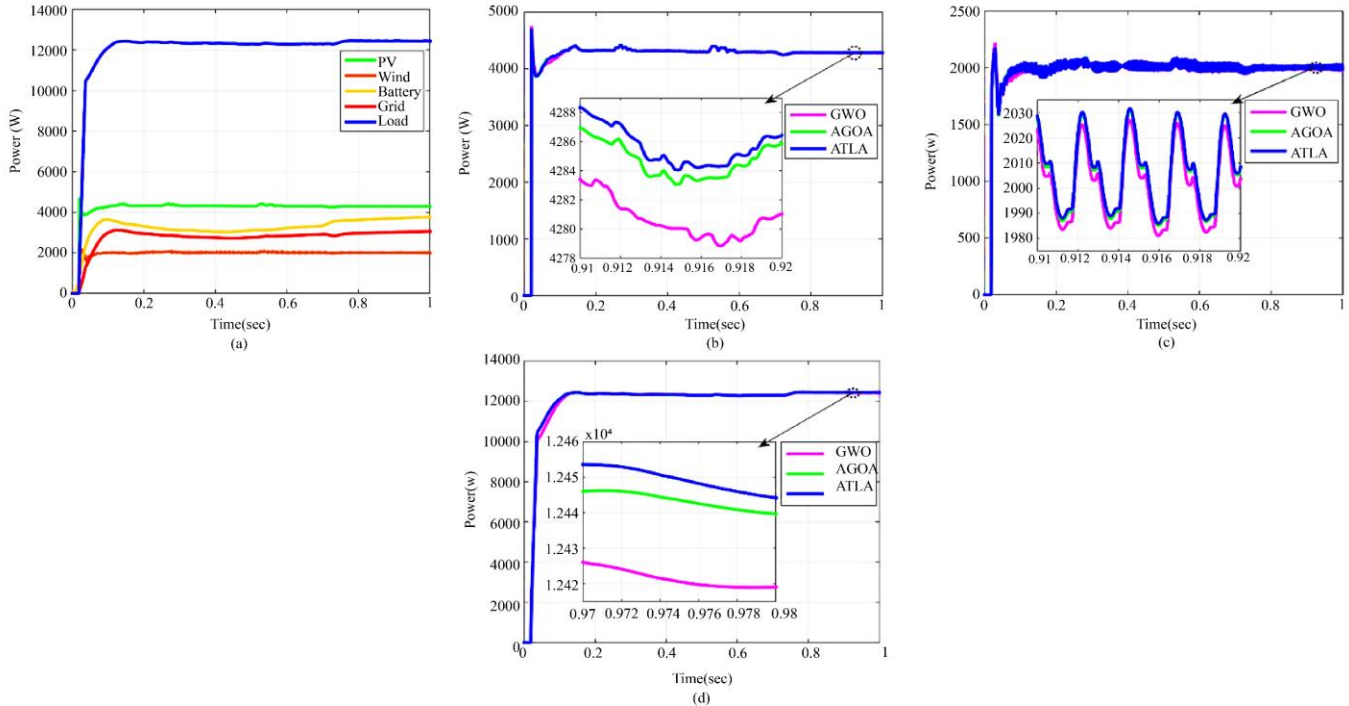


Fig. 10 Power outcomes under case-4 (a) Load Sharing, (b) PV power, (c) Wind power, (d) load power

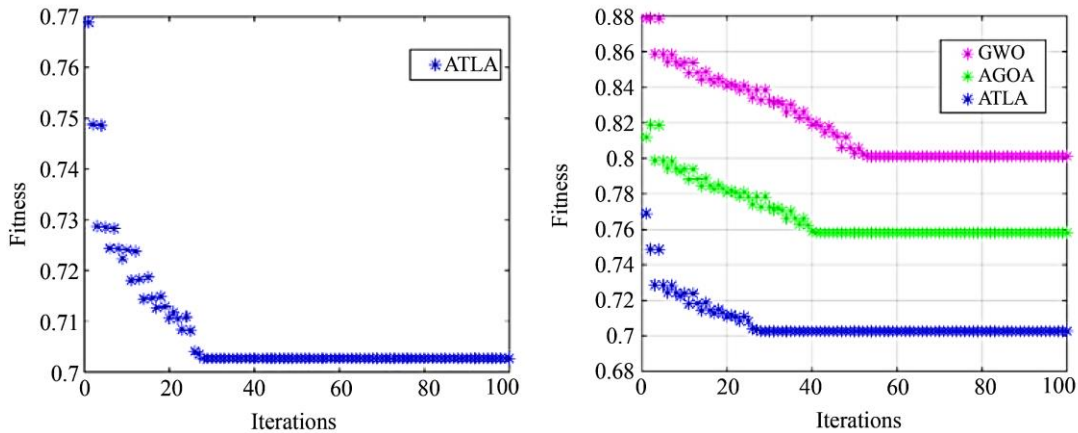


Fig. 11 Convergence characteristics of proposed and existing techniques (a) The ATLA control technique's fitness; (b) A comparison of the fitness of proposed and existing techniques

6. Conclusion

This work introduced the novel model of a grid-interfaced HRE-powered EVCS associated with modified SCBC for reducing the burden on the utility grid. The Artificial Transgender Longicorn Algorithm (ATLA) creates an effective control system and an appropriate controller to accomplish optimum power consumption. The recommended controller achieved the best energy management, robustness, and optimal utilization of power in EVCS by providing optimal switching to the converters and delivering accurate control signals. The recommended model is examined in MATLAB or Simulink, and the system's effectiveness is assessed using the tools at hand. The ATLA has been shown to be a very effective and optimistic control method for optimizing the suggested model in terms of both accuracy and

charge time when compared to other methods considered in this work. While the AGOA and GWO control approaches are competitive, they have a longer execution time than ATLA. From an accuracy point of view, ATLA performed better than the other competitive control techniques. This system model was examined using different cases, but only four of them are presented. The proposed controller enhanced the system's efficiency in the cases we considered. Therefore, the recommended control method for managing energy is successful and efficient.

Acknowledgments

The author(s) are conveying their thanks to Dr. B. Amarendra Reddy Garu for his support in analyzing the SCB converter.

References

- [1] Transport Uses 25 Percent of World Energy, the Maritime Executive, 2015. [Online]. Available: <https://www.maritime-executive.com/article/transport-uses-25-percent-of-world-energy>
- [2] US EPA. Climate Change Indicators: Greenhouse Gases. [Online]. Available: <https://www.epa.gov/climate-indicators/greenhouse-gases>
- [3] NASA. Weather Forecasting to Climate Change, NASA's AIRS Builds A Legacy, 2022. [Online]. Available: <https://climate.nasa.gov/news/3173/from-weather-forecasting-to-climate-change-nasas-air-builds-a-legacy/>
- [4] Lorenz Moosmann et al., The COP26 Climate Change Conference: Status of Climate Negotiations and Issues at Stake. [Online]. Available: <https://www.europarl.europa.eu>
- [5] 26th Conference of Parties (Cop26), Climate Change India's New Climate Targets: Bold, Ambitious and A Challenge for the World, 2021. [Online]. Available: <https://www.downtoearth.org.in>
- [6] Kejun Qian, Chengke Zhou, and Yue Yuan, "Impacts of High Penetration Level of Fully Electric Vehicles Charging Loads on the Thermal Ageing of Power Transformers," *International Journal of Electrical Power & Energy Systems*, vol. 65, pp. 102–112, 2015. [[CrossRef](#)] [[Google Scholar](#)] [[Publisher Link](#)]
- [7] Yonghua Song, Xia Yang, and Zongxiang Lu, "Integration of Plug-In Hybrid and Electric Vehicles: Experience from China," *In IEEE PES General Meeting*, pp. 1-6, 2010. [[CrossRef](#)] [[Google Scholar](#)] [[Publisher Link](#)]
- [8] [Online]. Available: <https://economictimes.indiatimes.com/industry/auto/auto-news/global-electric-vehicle-sales-up-109-in-2021-tesla-leads-with-14-share/articleshow/89590350.cms>
- [9] Qiyun Dang, "Electric Vehicle (EV) Charging Management and Relieve Impacts in Grids," *In Proceedings of the 9th IEEE International Symposium on Power Electronics for Distributed Generation Systems (PEDG)*, pp. 1-5, 2018. [[CrossRef](#)] [[Google Scholar](#)] [[Publisher Link](#)]
- [10] Qiuming Gong et al., "PEV Charging Control Considering Transformer Life and Experimental Validation of a 25 Kva Distribution Transformer," *IEEE Transactions on Smart Grid*, vol. 6, no. 2, pp. 648–656, 2015. [[CrossRef](#)] [[Google Scholar](#)] [[Publisher Link](#)]
- [11] Gaizka Saldaña et al., "Electric Vehicle Into the Grid: Charging Methodologies Aimed at Providing Ancillary Services Considering Battery Degradation," *Energies*, vol. 12, no. 12, 2019. [[CrossRef](#)] [[Google Scholar](#)] [[Publisher Link](#)]
- [12] Giri Rajanbabu Venkatakrishnan, Ramasubbu Rengaraj, and Nattamai Balasubramanian Prakash, "Optimally Manage the Energy Between Electric Vehicle Charging Stations and Electricity Distribution System: A Hybrid Technique," *International Journal of Numerical Modelling: Electronic Networks, Devices and Fields*, vol. 35, no. 1, pp. 1-23, 2022. [[CrossRef](#)] [[Google Scholar](#)] [[Publisher Link](#)]
- [13] Yannam Ravi Sankar, and K. Chandra Sekhar, "Hybrid Energy System for Smart DC Microgrid Using Optimized PI-Based CUK Integrated Boost DC-DC Converter," *SSRG International Journal of Electrical and Electronics Engineering*, vol. 10, no. 1, pp. 1-14, 2023. [[CrossRef](#)] [[Publisher Link](#)]
- [14] M F Zia, Elhoussin Elbouchikhi, and M. E. H. Benbouzid. "An Energy Management System for Hybrid Energy Sources-Based Stand-Alone Marine Microgrid," *IOP Conference Series: Earth and Environmental Science*, vol. 322, no. 1, 2019. [[CrossRef](#)] [[Google Scholar](#)] [[Publisher Link](#)]
- [15] H B Tambunan, P A A Pramana, and B S Munir, "Intermittent Renewable Energy Source (IRES) Model of Solar Energy in Cipayung Microgrid System," *Journal of Physics: Conference Series*. vol. 1402, no. 3, 2019. [[CrossRef](#)] [[Google Scholar](#)] [[Publisher Link](#)]
- [16] Sina Ibne Ahmed, Hossein Salehfar, and Daisy Flora Selveraj, "Grid Integration of PV Based Electric Vehicle Charging Stations: A Brief Review," *In 2022 North American Power Symposium (NAPS)*, pp. 1-6, 2022. [[CrossRef](#)] [[Google Scholar](#)] [[Publisher Link](#)]
- [17] Alex Caines et al., "The Grid Independence of an Electric Vehicle Charging Station With Solar and Storage," *Electronics*, vol. 10, no. 23, pp. 1-20, 2021. [[CrossRef](#)] [[Google Scholar](#)] [[Publisher Link](#)]
- [18] Gowthamraj Rajendran et al., "PSO-Based PI Controller for Voltage-Oriented Controller-Based Vienna Rectifier for Electric Vehicle Charging Stations," *In 2021 IEEE 19th Student Conference on Research and Development (Scored)*, pp. 356-361, 2021. [[CrossRef](#)] [[Google Scholar](#)] [[Publisher Link](#)]
- [19] G. Madhuri et al., "Fast Charging Electric Vehicle Using Fuzzy Logic Controller," *International Journal of Engineering Research & Technology*, vol. 9, no. 5, 2020. [[CrossRef](#)] [[Google Scholar](#)] [[Publisher Link](#)]
- [20] Musadg Zakaria, S. Anusha, and M. Sirisha, "A Multi-Mode Operating Tri Port Based Electric Vehicle Charging Station," *SSRG International Journal of Electrical and Electronics Engineering*, vol. 8, no. 8, pp. 9-15, 2021. [[CrossRef](#)] [[Publisher Link](#)]
- [21] Kisu Kim et al., "A Modified Series-Capacitor High Conversion Ratio DC–DC Converter Eliminating Start-Up Voltage Stress Problem," *IEEE Transactions on Power Electronics*, vol. 33, no. 1, pp. 8–12, 2018. [[CrossRef](#)] [[Google Scholar](#)] [[Publisher Link](#)]
- [22] J. Mahdavi, A. Emadi, and H.A. Toliyat, "Application of State Space Averaging Method to Sliding Mode Control of PWM DC/DC Converters," *In IAS'97, Conference Record of the 1997 IEEE Industry Applications Conference Thirty-Second IAS Annual Meeting*, vol. 2, pp. 820-827, 1997. [[CrossRef](#)] [[Google Scholar](#)] [[Publisher Link](#)]

- [23] Ameer A Kareim, and Muhamad Bin Mansor, "Efficiency Improvement of the Maximum Power Point Tracking (MPPT) for PV Systems Using Support Vector Machine Technique," *IOP Conference Series: Earth and Environmental Science*. vol. 16, no. 1, 2013. [[CrossRef](#)] [[Google Scholar](#)] [[Publisher Link](#)]
- [24] Xiaokuang Han et al., "ATLA: A Novel Metaheuristic Optimization Algorithm Inspired By the Mating Search Behavior of Longicorn Beetles in the Nature," *In IOP Conference Series: Materials Science and Engineering*, vol. 782, no. 5, 2020. [[CrossRef](#)] [[Google Scholar](#)] [[Publisher Link](#)]
- [25] P. Sobha Rani et al., "Adaptive Grasshopper Optimization Algorithm for Multi-Objective Dynamic Optimal Power Flow in Renewable Energy Integrated Microgrid," *International Journal of Intelligent Engineering & Systems*, vol. 15, no. 3, pp. 242-252, 2022. [[Google Scholar](#)] [[Publisher Link](#)]
- [26] I D Sara, and R Faulianur, "Grey Wolf Optimization for Track Maximum Power of Photovoltaic System in Multiple Peak Power Characteristics," *IOP Conference Series: Materials Science and Engineering*, vol. 523, no. 1, 2019. [[CrossRef](#)] [[Google Scholar](#)] [[Publisher Link](#)]
- [27] S.Surya, and S.Sivakumar, "A Novel Single-Phase Bidirectional Electric-Drive-Reconstructed Onboard Fuzzy Controlled Converter for Electric Vehicles," *SSRG International Journal of Electronics and Communication Engineering*, vol. 8, no. 4, pp. 1-4, 2021. [[CrossRef](#)] [[Publisher Link](#)]
- [28] Nihad Abdulkhudhur Jasim, and Majli Nema Hawas, "Modelling and Simulation of Microgrid Power System Including a Hybrid Energy Storage System," *IOP Conference Series: Materials Science and Engineering*. vol. 1105, no. 1, 2021. [[CrossRef](#)] [[Google Scholar](#)] [[Publisher Link](#)]
- [29] P Jyothi et al., "Renewable Energy Powered DC Charging System for Electric Vehicle," *Journal of Physics: Conference Series*, 2020. [[CrossRef](#)] [[Google Scholar](#)] [[Publisher Link](#)]